IEEE Access
Multidisciplinary ⋮ Rapid Review ⋮ Open Access Journal

Received February 1, 2021, accepted February 15, 2021, date of publication February 26, 2021, date of current version March 9, 2021.

Digital Object Identifier 10.1109/ACCESS.2021.3062385

Sleep Posture Recognition With a Dual-Frequency Cardiopulmonary Doppler Radar

JOHN E. KIRIAZI[1,2], (Member, IEEE), SHEKH M. M. ISLAM[1], (Member, IEEE), OLGA BORIĆ-LUBECKE[1], (Fellow, IEEE), AND VICTOR M. LUBECKE[1], (Fellow, IEEE)

[1]Department of Electrical Engineering, University of Hawai'i at Mānoa, Honolulu, HI 96822, USA
[2]Qualcomm Inc., San Diego, CA 92121, USA

Corresponding author: Shekh M. M. Islam (shekh@hawaii.edu)

This work was supported by the National Science Foundation under Grant IIS-1915738 and Grant CBET-1160326.

ABSTRACT While Doppler radar can be used to measure cardiopulmonary vital signs during sleep, meaningful diagnostic assessments are often subject to knowledge of a subject's changing sleep posture. The torso Effective Radar Cross Section (ERCS) and displacement magnitude were studied for 20 human subjects in three imitated sleep posture categories using a dual-frequency Doppler radar system in an exploratory examination of the feasibility of using radar to recognize body orientation. Box plot statistical analyses were performed for comparative assessment of ratio variations in ERCS and respiration depth for three different imitated sleep postures. The observed statistical trends and correlations were applied to a physical model to develop posture decision algorithms with initial supine posture data used as a reference. A single-frequency algorithm tracked postures without error for 90% of the subjects using 2.4 GHz data, and 80% using 5.8 GHz data. As accuracy limitations were complementary, a dual-frequency algorithm was developed which recognized postures without error for 100% of the subjects.

INDEX TERMS Doppler radar, radar cross-section, radar remote sensing, sleep posture, radar signal processing.

I. INTRODUCTION

Sleep is a biological imperative for humans, and quality of sleep plays an important role in ensuring people stay active, healthy, and energetic [1]. Irregular or insufficient sleep patterns increase daytime fatigue and have a proven relationship with chronic diseases, such as obesity and diabetes [1], [2]. One of the most common sleep disorders is sleep apnea, characterized by pauses in breathing during sleep that can increase the potential risk of serious diseases such as hypertension and bipolar disorder [1], [3], [4]. Various clinical investigations have demonstrated that the recoginition of key categories of posture assumed during sleep can serve as a diagnostic indicator for a variety of chronic diseases and can potentially aid in medical therapies [5]–[9]. The predominant categories of concern in sleep medicine are supine, prone, and side. For example, the avoidance of the supine posture (i.e., sleeping on one's back) can reduce the severity of sleep apnea [10] and reduce the risk of sudden infant death syndrome (SIDS) [11]. Also, pressure ulcers (i.e., bedsores) are a common medical ailment for bedridden patients, for which physicians or caregivers recommend adjusting postures every two hours [12]. Thus, there is significant value in an unobtrusive monitoring system which can recognize categories of sleep posture.

Prior related research has focused on recognizing sleep postures from cardiovascular signals extracted from electrocardiograms (ECG) [13]. However, this approach is contact based, requiring specialized instruments and trained professionals that can make the procedure too cumbersome and expensive for many applications. Video cameras have also been used to recognize sleep postures [14], however, the collection of video imagery introduces privacy issues, and the accuracy is hampered by obstructions such as bed covers [6]–[9]. Pressure-sensitive bedsheets with densely deployed textile sensors have been used to generate pressure map images, with machine learning (ML) classifiers used to recognize sleep postures [15]. However, when fully developed the sensor system must replace the user's simple bedding with a complex system that requires an active power supply, presents hygienic issues, affects comfort, and generally imposes a significant maintenance burden [6].

This paper examines an approach for recognizing three categories of sleep posture while simultaneously measuring

The associate editor coordinating the review of this manuscript and approving it for publication was Davide Comite.

diagnostic cardiopulmonary patterns using an unobtrusive and non-contact Doppler radar system. Previous applications of cardiopulmonary radar in the biomedical field have included monitoring cardiopulmonary-related motion characteristics of a single [16], [17] and multiple subjects [18]–[20]. Prior research also successfully demonstrated sleep monitoring [21] with CW [22]–[25], FMCW [26], [27], and UWB [28], [29]. While sleep applications of radar have included recognition of sleep stages (i.e., REM, non-REM) [24], [28], and apnea events [21], [25], [29], there have also been recent research efforts involving sleep posture recognition. Sleep posture recognition for chronic sleep disorder patients has been examined using Doppler radar with wavelet packet decomposition and a deep neural network [30]. The feature extraction method used was developed based on data collected in supine, prone, and side positions fed to deep neural network architecture, without employing a physical model. In contrast, the method proposed in this paper does not require a priori knowledge of patient signatures in prone and side positions and determines the subject's posture based on fundamental features that feed into a physical model which works beyond sleep disorder patients to track a full variety of healthy or ill subjects. Recently, frequency modulated continuous wave (FMCW) radar was applied with a multipath analysis of reflections used to distinguish sleep postures using a neural network model [31]. However, this method requires calibration data with subjects wearing accelerometers in different sleep postures in a fixed home environment (accuracy 94.1%). Furthermore, multipath is highly dependent on the physical environment including furniture or other people. When the neural network model was transferred to other subjects in different environments, accuracy was reduced to 86.7% and 83.7%, and the method was not effective for a prone subject.

In our prior research, real-time sleep monitoring using microwave Doppler radar was demonstrated for recognizing different obstructive sleep apnea events (apnea, hypopnea) [25]. However, patients were instructed to maintain their sleep postures to simplify the analysis, and the radar system focused solely on extracting breathing and heart patterns with posture changes considered an unwanted source of measurement interference. The potential for a similar sleep apnea monitoring system to be used to track and compensate for posture changes is considered in this paper. This approach is based on a physical model that does not depend on extensive learning of a particular subject in each posture of interest, or an unchanging physical environment. While the phase-modulated reflection in a physiological radar measurement is directly proportional to the subtle movement of the subject's chest surface due to cardiorespiratory activity, the power of the signal at the receiver is a measure of effective radar cross-section (ERCS) [32]. When subjects switch postures it affects the ERCS, as different parts of the body are exposed to the radar and those parts convey cardiopulmonary motion differently. Additionally, measured displacement varies with body orientation. This offers the potential to tailor sleep apnea

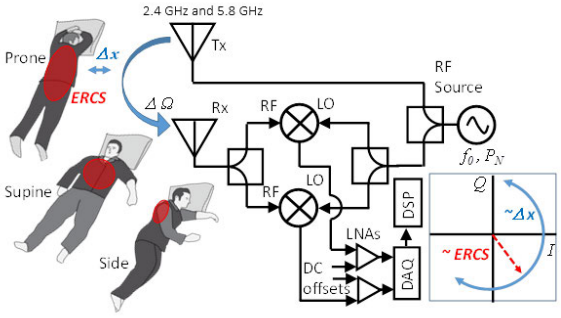

FIGURE 1. Concept and block diagram for continuous-wave Doppler radar system used to distinguish sleep postures during cardiopulmonary monitoring. I-Q phase varies with torso displacement while ERCS varies with sleep postures.

recognition to the known posture of the subject, even when that subject changes posture through the night. Also, respiratory tidal volume measurement depends on foreknowledge of subject posture [33], [34], and thus this too can be similarly tracked by the integration of ERCS and displacement measurements. Furthermore, the ERCS measurement itself can be used as an indicator of sleep apnea events [35].

The research presented here tests the hypothesis that a physiological radar system can accurately recognize changes in posture in a manner required for accurate assessment of cardiopulmonary motion with the same radar system, as illustrated in Fig. 1. Measurements previously taken on a single subject [32] showed a significant difference between the ERCS in the three sleep-type postures as well as between the respiration depth of a subject in prone and supine postures. However, the significance and repeatability of those results must be further examined by studying variations in a small sample population of subjects to explore whether the method is viable for supporting diagnostic measurements for varied patients in clinical studies of sleep apnea or other respiratory disorders. The fundamental theory introducing ERCS and its relationship to posture has been reported in a Ph.D. dissertation, along with details on subject testing and the basis for a posture determination algorithm [36]. The two frequencies used for the study, 2.4 GHz and 5.8 GHz, were chosen not only for the ease of use of the ISM band, but for the relationship between the wavelength and the target dimensions for each, and accociated benefits in measuremenmt accuracy. In this paper, the reported subject data is analyzed through box-plot statistics from which new insight is derived and a corresponding comparative analysis is presented. The introduction of visualized estimators and related statistical analyses revealed key distribution trends. These have resulted in a more effective single-frequency posture decision algorithm (by up to 20%), and a more robust dual-frequency decision algorithm. Ultimately, single frequency posture assessments worked without error for 90% of the subjects at 2.4 GHz, 80% at 5.8 GHz, and 100% using dual-frequencies.

The accuracy of the measurement system for this study was initially assessed using a mechanical target to estimate the system sensitivity to misalignment of the target with

respect to the radar transceiver. The radar employed two carrier frequencies to introduce diversity for ERCS measurements. Measurements carried out on twenty human subjects are then presented, and data statistics are used to show the trend by which the ERCS and torso displacement magnitude are correlated to changes in posture. Based on these results, a decision algorithm was developed to investigate the ability to automatically recognize the sleep-type posture of a subject. In this algorithm, it is assumed that initial measurements are taken while the subject is in a supine posture. By applying the proper thresholds and using a dual-frequency radar, this research demonstrates that such a system can differentiate whether a subject maintains a supine posture or switches to a prone or side posture.

II. SYSTEM ACCURACY ASSESSMENT

The Doppler radar system used here is designed for human cardiopulmonary sensing and configured to extract three main parameters for a moving target: ERCS, motion displacement magnitude, and rate of motion. The captured baseband signal traces an arc on the complex I-Q plot where the radius is proportional to the square-root of the ERCS. The angle scanned by the arc on the complex I-Q plot corresponds to the displacement magnitude of the moving target. The quadrature baseband signals are dc-coupled to the two-stage cascaded LNA's. The dc component in each signal is subtracted at the second stage where the amplified signal from the first stage is added to its dc estimate with negative polarity and correct scaling [37], [38]. The measurement system and I-Q concepts are illustrated in Fig. 1. In principle, the ERCS measurement using Doppler radar is based on detecting phase modulation caused by a moving target. Since the motion is in the direction of the transceiver, the target range is also modulated by the displacement leading to a variation in the power of the returning wave. For a small displacement away from the center position, the amplitude modulation can be neglected but the angle scanned by the arc introduces an ambiguity in estimating the arc radius. On the other hand, a large target displacement lets the arc cover a larger part of a circle, but the amplitude modulation introduces some deformation to the arc and affects the radius estimation accuracy. The system used for this study employs two frequencies, 2.4 GHz, and 5.8 GHz, as using two carrier frequencies introduces diversity in the ERCS measurements. Table-1 lists the different components used for the Doppler radar system. Fig. 2 illustrates the antenna board platform used in this experiment. The setup has separate but identical transmitting and receiving antennas. Given that the target range is limited by the height of the ceiling, low frequencies are more likely to satisfy the wave-planarity condition of far-field measurements. Therefore, the differences in curvature between the front and back of the body become more detectable. On the other hand, high frequencies pull the target closer to the optical region of electromagnetic scattering where differences in size are more accurately detected. The target size effectively changes when the subject rolls to a side posture.

TABLE 1. Doppler radar system specifications.

Item	Model/Specification
Antenna Power splitters (0°) Power splitter (90°) Mixers	Antenna Specialist ASPPT 2998 Mini-circuits-ZFC-2-2500 (x2) Mini-circuits-ZX10Q-25-St Mini-circuits-ZFM 4212 (x2)
Transmitted power	10 dBm
Antenna gain	8.0 dBi
Radar Bandwidth	2.4-2.415 GHz, 5.8-5.82 GHz
Center Frequency	2.41 GHz, 5.81 GHz
Maximum range	2.5 meters
Directivity	E-plane: beamwidth 60° H-plane: beamwidth 80°

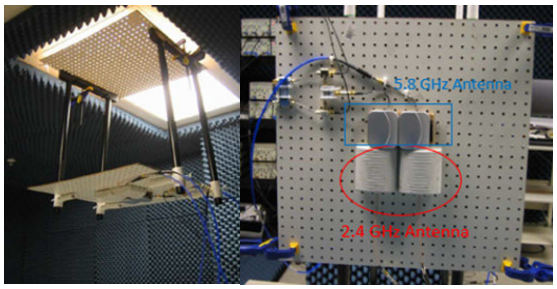

(a) (b)

FIGURE 2. Ceiling-mounted antenna platform for radar sleep posture measurements (a). The platform used separate but identical transmitting and receiving antennas, including two ASPPT 2998 panel antennas for 2.4 GHz (red circle) and two Wi-Fi antennas for 5.8 GHz (blue rectangle), and was mounted vertically for the short-range mechanical mover measurements (b).

In order to establish validity for the measured quantities, system accuracy was tested using a metallic spherical object in a setup similar to the one presented in [32]. The target used was a metallic hemisphere with a diameter $d = 24.5$ cm. From Mie series solution for perfectly conducting spheres [39], the target lies toward the end of the resonance region at 2.4 GHz and at the beginning of the optical region at 5.8 GHz. The size of the hemisphere is also comparable to the dimensions of the average human torso.

A. ERCS MEASUREMENT ACCURACY

The accuracy by which ERCS is measured depends on the system sensitivity to the target alignment. In this experiment, the target was measured at three different positions. First the target was laterally aligned with the transceiver. The baseband signals were recorded while the target was oscillating in the axial direction. Then the process was repeated with the target shifted laterally by two centimeters to the left and two centimeters to the right. The target was initially put in motion using a mechanical mover with a 10-mm displacement magnitude. The mechanical mover simulated chest surface movement which typically ranges from 4-12 mm with a frequency range of 0.2-0.34 Hz (12 to 20 breaths per minute). The arc

TABLE 2. Arc radius estimation for target with 10-millimeter motion amplitude at three lateral positions.

Position	2.4 GHz A[V]				5.8 GHz A[V]			
	med	mean	max	std	med	mean	max	std
Aligned	4.26	4.25	4.29	0.017	1.45	1.45	1.46	0.007
Offset L	4.26	4.26	4.30	0.018	1.34	1.34	1.36	0.006
Offset R	4.32	4.31	4.44	0.050	1.28	1.28	1.30	0.006

TABLE 3. Arcs radius estimation for target with 5-millimeter motion amplitude at three lateral positions.

Position	5.8 GHz A[V]			
	med	mean	max	std
Aligned	1.25	1.25	1.28	0.017
Offset L	1.26	1.26	1.28	0.012
Offset R	1.22	1.21	1.23	0.012

TABLE 4. Displacement magnitude and rate estimation for target with 10-millimeter motion amplitude at three lateral positions.

Position	2.4 GHz			5.8 GHz		
	ΔΩ [deg]	Δx [cm]	Rate [rpm]	ΔΩ [deg]	Δx [cm]	Rate [rpm]
Aligned	66.2	1.149	18.0	140.1	1.006	17.9
Offset L	66.8	1.159	17.9	145.0	1.041	17.9
Offset R	65.5	1.137	17.9	146.1	1.049	17.9

TABLE 5. Displacement magnitude and rate estimation for target with 5-millimeter motion amplitude at three lateral positions.

Position	5.8 GHz		
	ΔΩ [deg]	Δx [cm]	Rate [rpm]
Aligned	76.1	0.547	18.0
Offset L	74.4	0.535	18.0
Offset R	75.7	0.544	18.0

radius was calculated using a center estimation algorithm [40] and the resulting statistics are presented in Table 2. For 2.4 GHz the mean arc radius was 4.25 V in the aligned position, 4.26 V with a two-centimeter shift left, and 4.31 V with a two-centimeter shift right. The maximum error caused by the displacement offsets was 1.4%. Using 5.8 GHz, the mean arc radii were 1.45 V, 1.34 V, and 1.28 V, respectively, giving an error of 13%.

Another set of measurements was obtained at 5.8 GHz but with the target, motion amplitude reduced to 5 mm. The results are presented in Table 3. In this case, the mean arc radius was 1.25 V for the aligned position, 1.26 V for the two-centimeter shift left, and 1.21 V for the two-centimeter shift right. The corresponding error was only 4%, indicating that the electrical length of the displacement affects the ERCS measurement accuracy. The dependence of ERCS accuracy on target displacement was evaluated by comparing the mean arc radius obtained with 10-mm and 5-mm motion magnitudes, 1.45 V compared to 1.25 V. This emulated the scenario of repeated measurement of the same target but with different motion magnitudes, and the corresponding error was 16%. In human testing, it is expected that the subject can be laterally aligned with plus or minus two-centimeter accuracy. The torso displacement during respiration can range from a few millimeters up to about three centimeters. Therefore, accuracy in estimating the arc radius is generally expected to be about 15% which has been proven satisfactory for posture assessment.

B. DISPLACEMENT MEASUREMENT ACCURACY

By measuring the scanned arc angle, $\Delta\Omega$, the displacement was calculated using $\Delta x = \lambda \cdot \Delta\Omega / 4\pi$. Table 4 and Table 5 show the values of Δx obtained using a mechanical displacement of 10 mm and 5 mm, respectively. For the 10-mm oscillation displacement, the 2.4 GHz measurements had a maximum discrepancy when the target was at a two-centimeter offset to the left. The reading for this measurement was 1.16 cm. Hence, the maximum error was about 16%. At 5.8 GHz, the maximum error was reduced to 5%. But when the target oscillation was 5 mm in amplitude, from Table 4, the error increased to 10%. This indicates that greater accuracy is expected for electrically larger target displacement despite leading to a variation in the power of the returning wave. For a small displacement away from the center position, the amplitude modulation can be neglected but the angle scanned by the arc on the complex I-Q plot is also small. Considerably small arcs introduce ambiguity in estimating the arc radius. On the other hand, a large target displacement allows the arc to cover a larger part of a circle, but the amplitude modulation introduces some deformation to the arc and affects the radius estimation.

C. RATE MEASUREMENT ACCURACY

In these tests, the mechanical target was set to swing with a 0.3-Hz oscillation frequency. Therefore, the motion rate was 18 rotations per min. The rotation rate was measured by counting the number of cycles detected in the in-phase or quadrature baseband signal as long as it was not at a "null" point. From Table 4 and 5, the measured rate in all cases was approximately 18 rpm with a maximum error of 0.5%. Hence, for human subject testing, accurate respiration rate can be expected regardless of respiration depth and for both the 2.4 and 5.8 GHz systems.

III. HUMAN SUBJECTS TESTING

A study of the cardiopulmonary characteristics for multiple human subjects was conducted under IRB protocol number 14884 of the Committee of Human Studies at the University of Hawaii. The rf transmission power for these studies was generally less than for typical WiFi router exposure. A total of twenty subjects, 6 females and 14 males, were included in the study. The physical characteristics of this population are shown in Table 6. The ages of the participants ranged from 22 to 75 years. The body mass index varied from 19 to 31.8 kg/m^2 where 8 subjects had normal weight, 11 were overweight, and one was obese. The chest

TABLE 6. Subjects physical properties.

No.	Age	Gen	Ht [cm]	Wt [kg]	BMI [kg/m^2]	CB_{max} [cm]	CB_{min} [cm]	CD_{max} [cm]	CD_{min} [cm]	WC_{max} [cm]	WC_{min} [cm]	CC_{max} [cm]	CC_{min} [cm]
01	30	M	164.5	86.1	31.8	34	32	24	22	100	97.5	102.5	99
02	33	M	174	80.3	26.5	34	32	26	24	100	98	104.5	102.5
03	45	M	172	82.1	27.8	34	32	26	24	99.5	97	106	102
04	42	F	172.7	62.3	20.9	28	25	21	19	81	76	93	87
05	24	M	175	61.3	20	28	27	21	20	73.5	73	82.2	81.1
06	23	F	155	45.7	19	26	25	19	18	70	66	82	78
07	25	M	179	77.2	24.1	33	31	21	20	89	87	98	95.6
08	31	M	177.8	79.4	25.1	34	32	22	20	96	93.5	103	100.5
09	63	F	164	66.8	24.8	35	30	21	20	93	85	101	97
10	22	M	171	80.8	27.6	31	30	24	22	92	90	98	94
11	41	F	164	61.3	22.8	28	26	20	18	84	82	95	91
12	24	M	180.3	86.1	26.5	33	30	22	20	96	95	98	94
13	26	M	186	87.5	25.3	35	34	21	20	98.5	96	105	103
14	27	M	182.8	77	23	33	31	20	18	83	82	98.5	95.5
15	75	F	162	67	25.5	29	28	21	20	87	84	91	88
16	28	M	182.8	87.3	26.1	33	30	23	20	88.5	86	102.5	95
17	33	F	178	84.8	26.8	34	32	24	21	90	85	104	98
18	27	M	188	104.8	29.65	34	32	25	23	98	96.5	108	104.5
19	35	M	185	75.6	22.1	31	30	21	19	87	85	97	95.5
20	29	M	167	70.1	25.1	31	29	23	21	95	93	98	96

CB is the chest breadth, CD is the chest depth, WC is the waist circumference, and CC is the chest circumference. The maximum values correspond to maximum inhalation while the minimum ones correspond to maximum exhalation.

breadth displacement from maximum inhalation to maximum exhalation ranged from 1 to 5 cm. The maximum chest depth displacement ranged from 1 to 3 cm. For sedentary breathing patterns, the maximum chest displacement ranged from 1 to 5 cm (normal to front chest surface) and chest breadth displacement ranged from 1 to 8 cm (parallel to chest surface) [41], [42]. The maximum chest breadth is the reading at maximum inhalation while the minimum breadth is at maximum exhalation. The maximum chest breadth is a bit larger than chest displacement, which is due to the complex nature of chest expansion during respiration. Each subject was measured in three recumbent postures: supine, prone, and side. Within an anechoic chamber, each subject was instructed to wear effort belts and a finger pulse strap used for reference measurements and then lay down on a flat horizontal surface. The transceiver antennas were suspended above the subject using the ceiling of the chamber at a range of 2.05 m, referred to as the bed surface. A total of six measurements were taken for every subject. First, the subject assumed the supine posture while received signals were recorded for 90 seconds with the system operating at one of the two RF frequencies. With the same posture maintained, the system was switched to the other operating frequency and the new signals were recorded, also for 90 seconds. The subject was then asked to change posture and the same procedure was repeated for prone and side postures. All experiments were performed when subjects were fully clothed but not covered by any blankets. Prior research has demonstrated the efficacy of Doppler radar in this frequency range when used for extracting vital signs when subjects were covered with a bed sheet or quilt [24]. One of the major challenges in radar-based unobtrusive sleep posture recognition results from the motion noise produced by the random body or involuntary limb movement. However, successful Doppler radar respiration sensing during random body movement has been demonstrated in prior work [43]–[45]. In the associated methodology, random body movement was mitigated by utilizing three different strategies, including: (1) phase compensation at the Doppler RF front-end [45], (2) phase-compensation for baseband complex signals [44], and (3) cancellation during demodulation [43]. Furthermore, in long-duration studies tracking of cardiopulmonary characteristics is most useful when done during sedentary instances as a lack of knowledge of the exact type of motion during each non-sedentary instance makes it difficult to judge the diagnostic merit for such measures. For this, methods have been demonstrated for distinctly recognizing sedentary conditions and using only those for comparative assessments, and it has been shown that such instances are very common between instances of random motion [46]. These approaches can be applied as needed with the posture tracking methods and the exact approach would likely be optimized for the application.

IV. RESULTS AND STATISTICS

For each human subject, the baseband signal recorded at every measurement scenario was analyzed to extract the relative ERCS and the absolute torso displacement magnitude. The time-domain signal was segmented into full respiration cycles [32]. Each segment traced an arc on the complex I-Q plot where the radius was estimated using a center estimation algorithm. The segment-leading to maximum arc radius was selected then the value was refined using the circle fitting algorithm. Table 7 shows the resulting arc radius at every posture and frequency.

The square of the radius is proportional to the ERCS of the torso at the corresponding orientation. The angle scanned by the arc leads to the torso displacement magnitude during respiration, shown in Table 7 at every posture and frequency.

TABLE 7. Displacement magnitude and estimated arc radius at 2 meters for two different frequencies (2.4 GHz and 5.8 GHz).

No.	Supine Δx [cm] and A [V]				Prone Δx [cm] and A [V]				Side Δx [cm] and A [V]			
	2.4 GHz		5.8 GHz		2.4 GHz		5.8 GHz		2.4 GHz		5.8 GHz	
	Δx [cm]	A [V]	Δx [cm]	A [V]	Δx [cm]	A [V]	Δx [cm]	A [V]	Δx [cm]	A [V]	Δx [cm]	A [V]
01	1.50	3.97	1.15	2.63	0.46	11.41	0.35	5.19	0.58	4.27	0.44	1.33
02	0.78	5.72	0.86	6.34	0.38	12.07	0.74	3.89	0.35	3.56	0.29	2.89
03	1.13	2.90	0.93	5.11	0.43	5.70	0.40	4.75	0.53	1.09	0.68	0.94
04	1.29	5.14	1.40	3.14	0.29	6.72	0.27	2.93	0.59	2.11	1.13	0.37
05	1.19	1.16	0.65	4.65	~~2.04~~	~~0.56~~	0.31	3.94	0.47	1.87	0.47	0.75
06	1.24	2.75	1.35	0.87	0.54	1.91	0.46	0.70	1.20	0.46	0.34	0.93
07	1.91	1.83	1.06	2.69	0.69	8.90	0.37	5.55	0.61	2.27	0.56	0.98
08	0.77	3.07	0.44	5.70	0.45	8.36	0.64	3.52	0.75	0.89	0.55	0.96
09	0.89	2.84	0.84	3.94	0.72	3.94	0.41	4.04	1.12	0.54	0.25	2.39
10	1.66	0.67	0.94	1.61	0.86	3.46	0.81	1.70	1.68	0.57	0.85	0.38
11	1.25	1.64	1.19	1.09	0.29	9.24	0.31	3.08	0.52	1.19	0.48	0.59
12	~~2.26~~	~~1.12~~	1.02	4.08	0.58	6.06	0.28	7.44	0.97	0.67	0.66	0.51
13	0.80	3.39	1.13	1.32	0.60	6.01	0.38	5.75	0.66	1.45	1.03	0.26
14	1.00	2.47	0.33	6.84	0.38	5.10	0.25	2.54	1.05	0.41	1.05	0.32
15	0.73	2.37	1.06	0.74	0.82	1.75	0.52	1.51	1.30	0.21	0.52	0.37
16	0.98	2.29	0.47	7.98	0.57	10.65	0.37	4.31	1.15	0.60	0.42	1.18
17	2.43	2.86	2.11	4.25	1.75	1.86	0.37	9.97	2.17	1.21	1.40	2.18
18	1.81	1.32	0.65	6.72	0.22	13.91	0.19	10.34	1.21	0.66	0.52	0.74
19	0.93	2.17	0.50	7.26	0.29	8.85	0.28	4.61	~~2.35~~	~~0.19~~	0.52	0.90
20	1.16	2.27	0.61	3.80	0.30	10.06	0.37	5.64	1.72	0.75	0.44	2.88

The arc radius A is estimated by selecting the segment of data having the maximum arc radius using center estimation algorithm then applying the circle fitting to that segment to recalculate the radius value. The displacement magnitude Δx is estimated by selecting the segment of data having the maximum arc radius using center estimation algorithm then applying the circle fitting to that segment to recalculate the angle spanned by the arc and hence the displacement magnitude. For a few data points where the signal to noise level was insufficient to make a reliable reading (shown with strike through) the measurements were stricken from the analysis.

The entries marked with strikes in the tables indicate discarded data, where the signal to noise ratio was insufficient to resolve arc and radius features with adequate resolution. These included data corresponding to distorted arcs where the estimated circle radius was too small to contain the arc. These cases are usually associated with an estimated displacement magnitude that is larger than the physically measured chest depth span of the subject in standing position shown in Table 5. The results in table 6 indicate changes in measured ERCS and estimated torso displacement magnitudes for three sleep-type postures, for any individual subject. The trend by which both quantities vary with posture can be understood through statistical analyses of the relationship between the measured parameters at two different postures. Taking supine as a reference, the first set of parameters to be studied consisted of the ratios of the arc radius in prone and side postures to that in supine. The second set was the ratios of the torso displacement magnitudes. Statistical analyses were applied to the results captured using each operating frequency, separately.

A. ERCS VARIATION

The value of the estimated ERCS, and hence the arc radius, vary between subjects due to several factors inherent to the individual being measured. These include the size of the subject, the curvature of the body surface, the body fat, and the respiration motion characteristics. In addition, there is variation due to the tolerance in the measurement itself. By taking the ratio of the arc radius in prone to that in supine, the resulting quantity was normalized with respect to the subject physical characteristics. By obtaining the distribution over all subjects, the tendency of this ratio to cluster around a certain value was examined, as well as repeatability among the population under study. Similarly, the ratio of the arc radius in side posture with respect to supine was calculated for every subject with similar analyses applied. For the 2.4 GHz measurements, the far-field conditions were met. The arc radius ratio distribution box plot of prone-to-supine ratio and side-to-supine ratio is illustrated in Fig. 3. It can be observed that the majority of the subject back-to-front posture ratios have broader distribution than side-to-front postures. The median for prone-to-supine arc radius ratio distribution was 2.3, first quartile was 1.4, and third quartile was almost 4.8. This implies that the ERCS of the back of the body tends to be at least 4 times larger than that of the front (Table-2). For the side-to-supine arc radius ratio distribution the median was 0.35, first quartile was 0.25, and third quartile was almost 0.75, which clearly illustrates the variability of dispersion of the two simulated sleep posture ERCS-ratio data measurements. The overall mean and standard deviation of the prone-to-supine arc radius ratios were 3.2 and 2.46, respectively. For the side-to-supine ratios, the mean was 0.54 and the standard deviation was 0.41.

Unlike supine and prone postures where the size of the moving surface exposed to the incident wave was similar, in the side posture the size of the exposed surface was relatively reduced. At 2.4 GHz and depending on the size of the subject, the reduction could be such that the target fell in the resonance region of interaction with the electromagnetic wave, resulting in ERCS fluctuation that was not proportional to size. But for the majority of the subjects in this test, the ERCS of the side was smaller than that of the front and on

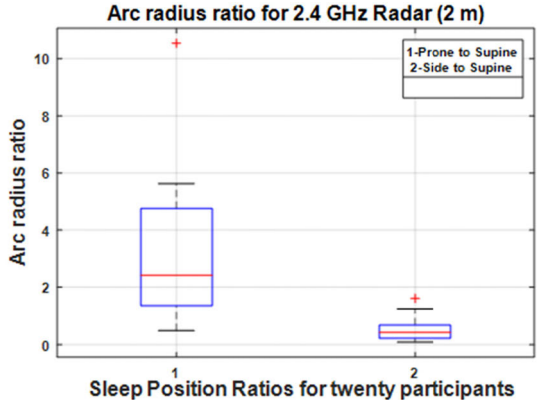

FIGURE 3. Box and whisker plot of arc radius ratios with respect to supine posture at 2 meters with a 2.4 GHz carrier. The interquartile range (IR) (two boundaries of box) clearly illustrates the variability between (prone to supine IR = 3.4, side to supine IR = 0.5) the two distributions.

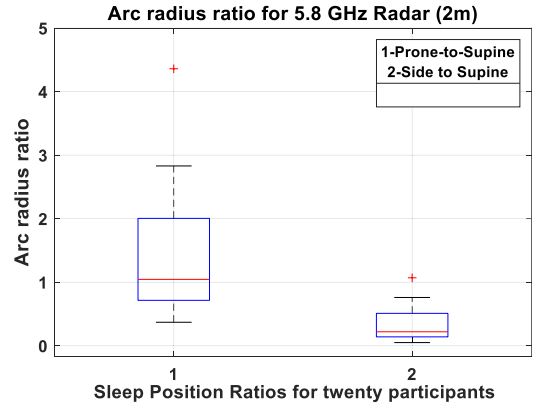

FIGURE 4. Box and whisker plot of arc radius ratios with respect to supine posture at 2 meters with a 5.8 GHz carrier. The interquartile range (IR) (two boundaries of box) clearly illustrates the variability between (prone to supine IR = 1.25, side to supine IR = 0.3) the two distributions.

average tended to be a quarter of the ERCS of the front. The average ERCS ratios of prone-to-supine and side-to-supine are strongly consistent with the proposed half-cylinder model introduced in [47].

At 5.8 GHz, the radiation far-zone condition was strongly met but the dimensions of the target led to spherical wave measurements in the supine and prone postures. In the side posture, since the exposed area of the body was already smaller, the wave front tended to be planar especially along the chest depth dimension. The box plot of the prone-to-supine and side-to-supine ratio distributions for the 5.8 GHz carrier at 2 m is shown in Fig. 4. The median for the prone-to-supine arc radius ratio was 1.1, the first interquartile was 0.75, the third interquartile was 2, and the interquartile range was 1.25. For the side-to-supine radius ratio distribution, the median was almost 0.23, first quartile was 0.2 and third quartile was 0.5. The interquartile range was almost 0.3. With 5.8 GHz carrier, the overall mean and standard deviation of the prone-to-supine arc radius ratios were 1.44 and 0.97, respectively. For the side-to-supine ratios, the mean was 0.35 and the standard deviation was 0.27.

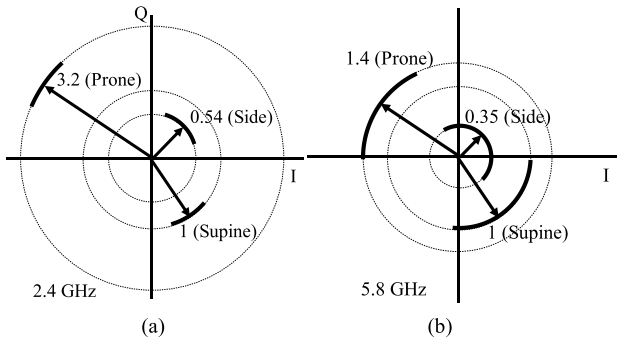

FIGURE 5. Normalized average arc radius I/Q plots for prone, supine, and side postures, at (a) 2.4 GHz, (b) 5.8 GHz.

The two box plots in Fig. 2 and 3 clearly illustrate that the variability of dispersion of the arc radius ratio distributions at two different frequencies have the same trend in distribution size in terms of the interquartile range. A summary of distinct arc radius variation with posture is illustrated in Fig. 5.

B. DISPLACEMENT MAGNITUDE VARIATION

The data collected in Table 7 shows that the respiration depth is altered when a subject changes posture from supine to prone. For instance, at 2.4 GHz the measured displacement of subject #01 in the prone posture was 0.46 cm compared to 1.5 cm in supine. This implies that the respiration depth was reduced approximately by a factor of 3. Similarly, in the side posture the measured displacement was 0.58 cm, which is also smaller than that in supine, this time by a factor of 2.5. The respiration depth reduction in the prone posture is expected as the body weight resists torso motion during respiration compared to relatively unhindered respiration in supine. But for the side posture, while one side of the body is facing the hard-supporting surface, the other side is moving upward with a displacement proportional to the chest breadth span. From Table 5, the span of the chest breadth in standing position is equal to that of chest depth for most of the subjects. Therefore, the respiration depth in supine will be maintained as a reference. The amount of reduction in prone respiration depth and how the displacement magnitude in the side posture compares to supine can be examined through statistical analyses. Thus, the displacement magnitude ratio was the second parameter investigated.

As demonstrated in the system calibration and accuracy assessment, the spherical target displacement was measured with a tolerance of 16% at 2.4 GHz and 10% at 5.8 GHz. Although at 5.8 GHz the target is located in the spherical-wave zone, the displacement measurement is more accurate because the target is positioned further in the radiation far-zone while the amount of displacement is independent of the target shape. Therefore, the system sensitivity to target surface curvature is not impacting the displacement measurement as long as the target is far from the radiator in terms of the number of propagation wavelengths.

For 2.4 GHz the ratio of the prone-to-supine and side-to-supine respiration depth ratio was calculated, and the

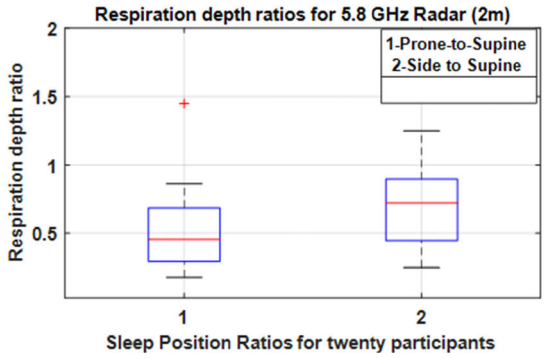

FIGURE 6. Box and whisker plot of respiration depth ratios with respect to supine posture at 2 meters with a 2.4 GHz carrier. The interquartile range (IR) (two boundaries of box) clearly illustrates the variability between (prone to supine IR = 0.35, side to supine IR = 0.68) the two distributions.

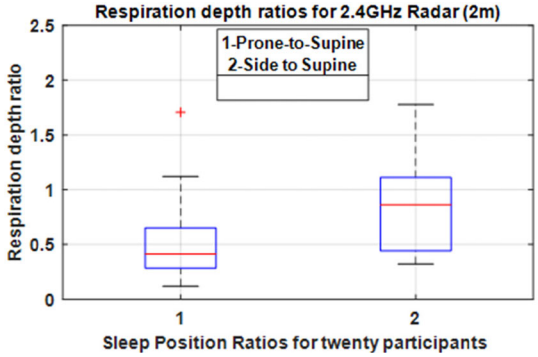

FIGURE 7. Box and whisker plot of respiration depth ratios with respect to supine position at 2 meters with a 5.8 GHz carrier. The interquartile range (IR) (two boundaries of box) clearly illustrates the variability between (prone to supine IR = 0.33, side to supine IR = 0.43) the two distributions.

box plot distribution is shown in Fig. 6. The median for prone-to-supine ratio was 0.4, first quartile was 0.3 and third quartile was 0.65. The interquartile range in the distribution was 0.35. The overall average of prone to supine ratio was calculated as 0.48 and the standard deviation as 0.25, confirming that for the average human subject tested the respiration depth while prone was less than that in supine by a factor of 2. Similarly, for the side-to-supine respiration depth ratio, the median was 0.85, first quartile was 0.42 and third quartile was 1.1. The interquartile range of the distribution was 0.68. The overall average was 0.83 and the standard deviation was 0.42. The majority of the subjects generally had side-to-supine ratios in the vicinity of unity. As a result, there should be no significant difference expected for the displacement magnitude in side posture compared to that in supine for the average human subject.

Similarly, a box plot of prone-to-supine and side-to-supine respiration depth ratio using 5.8 GHz is shown in Fig. 7. The median of the prone-to-supine ratio was 0.45, the first quartile was 0.32 and the third quartile was 0.65. The interquartile range was 0.33. The mean of the distribution was 0.52 and standard deviation was 0.31. These results are in agreement with those obtained at 2.4 GHz confirming that the respiration depth in the prone posture tends to be half that in supine for the average human subject. Similarly, the side-to supine depth ratio median was 0.7, first quartile was 0.42 and third quartile was 0.85. The interquartile range was 0.43. The mean of the distribution was 0.8 and the standard deviation was 0.63. This also aligns with previous results obtained at 2.4 GHz indicating a considerably small difference in the torso displacement magnitude in the side posture with respect to supine. A simple t-test was performed in Matlab to assess the significance of differences between the two different data sets (prone-to-supine and side-to-supine). The results showed that the t-test rejects the null hypothesis with a significance interval of 99% which also validates the difference between two posture data sets.

V. POSTURE RECOGNITION

In a likely practical application of cardiopulmonary remote sensing, a patient who is initially in the supine posture would be continuously monitored by sensors attached to the ceiling and pointing downward. During that time, the patient physiological characteristics would be logged. These include heartbeat, respiration rate, ERCS and torso displacement magnitude. Over extended monitoring, the patient is expected to roll in bed, changing orientation with respect to the sensors while measurements are proceeding. Tracking posture not only facilitates sleep analysis but could also allow respiratory tidal volume to be deduced from the other measurements [32], [33].

The previous data statistics assessed the amount of variation expected for an average human when rolling in bed from a supine posture to a prone or side posture. From these results, thresholds can be determined to set the boundary between the values corresponding to each assumed sleep posture. It is then possible to develop a decision algorithm to detect whether the subject has changed posture.

The reference inputs required by the algorithm are the measured parameters in the supine posture. Once the reference readings are obtained, the system can periodically assess the ERCS and displacement magnitude. In every cycle, measurements are compared to those in the supine posture, and resulting ratios are compared against boundary thresholds. The tolerances in ERCS and displacement measurements from Section II provided the boundary from which the thresholds for maintaining the supine posture were derived. The thresholds used to resolve the prone and side postures were determined based on a statistical analysis of the twenty subject study and selected for maximum likelihood of a correct decision.

Fig. 8 depicts flowcharts of the proposed single and dual frequency decision algorithms, where Ar and Dr denote ratios of arc radii and displacement magnitudes, respectively. Applying this algorithm to the population of subjects, the readings of prone-to-supine were first entered, and the corresponding decisions examined. Then the same procedure was followed for the side-to-supine readings. Two subjects

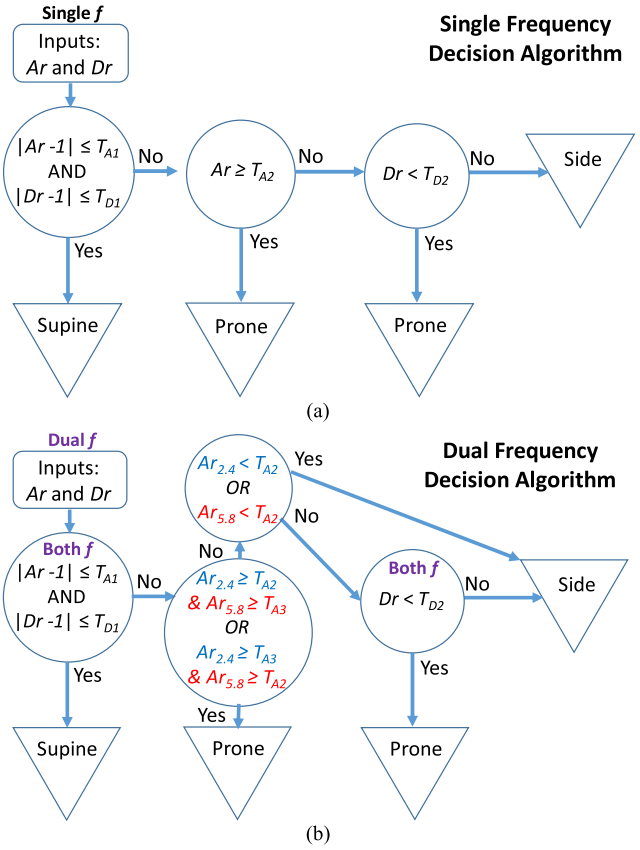

FIGURE 8. Single and dual frequency flowcharts of decision algorithms used to determine subject sleep posture based on arc radius ratio (*Ar*) and displacement magnitude ratio (*Dr*) threshold tests. Single frequency decision is based on two threshold assessments for both *Ar* and *Dr* (a), while the dual frequency decision introduces a third threshold test for both *Ar* and *Dr* (*b*).

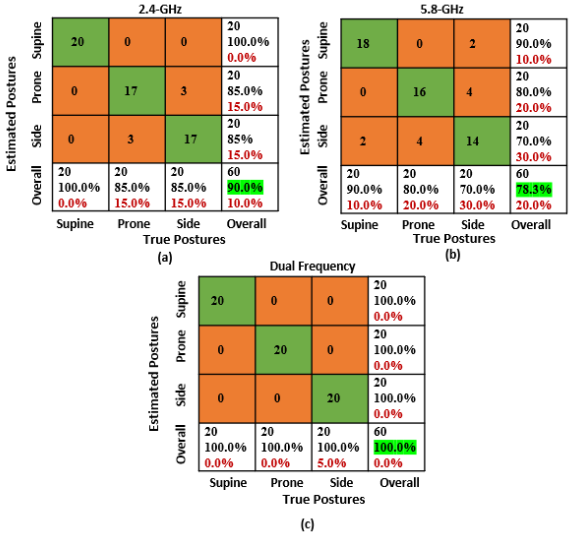

FIGURE 9. Confusion matrix for posture assessments using 2.4 GHz only (a), 5.8 GHz only (b), and a dual-frequency measurement (c). With the incorporation of interquartile range statistics for arc lengths, on average postures for 90% of subjects were assessed correctly using 2.4 GHz (15% false classification for side postures and 10% false classification for prone postures), and on an average 80% were correctly assessed using 5.8 GHz. Utilizing dual frequencies all subjects were correctly assessed.

were excluded from the prone-to-supine data because the result for the 2.4 GHz arc radius was discarded in either the prone or supine data, as shown in Table 6. Similarly, two subjects were excluded from the side-to-supine data.

To assess accuracy of single-frequency systems, decision algorithms were developed for each of the 2.4 GHz and 5.8 GHz radars, as shown in Fig 8(a). From statistical calculations based on an initial analysis [36] the arc radius ratio thresholds used for 2.4 GHz were $T_{A1} = 0.014$ and $T_{A2} = 0.5$, and the displacement ratio thresholds were $T_{D1} = 0.16$ and $T_{D2} = 0.35$. For 5.8 GHz they were $T_{A1} = 0.16$ and $T_{A2} = 0.3$, and the displacement ratio thresholds were $T_{D1} = 0.10$ and $T_{D2} = 0.35$. Using 2.4 GHz alone, 3 out of 18 subjects in side posture were erroneously assessed as prone (subjects 1, 7, and 18) and one prone subject was incorrectly assessed as side (subject 17), thus functioning without error on 78% of the subjects. Using 5.8 GHz alone, there was an increase in errors as the algorithm resulted in 8 wrong decisions out of 20 for the side posture (subjects 1, 2, 6, 9, 11, 15, 17, and 20), thus functioning without error on 60% of the subjects. Box-plot statistics provide enhanced insight into the subject data dispersion. Using the resulting interquartile ranges for the arc lengths at each frequency the efficacy of the decision algorithms was significantly increased. Using $T_{A2} = 1.25$ for 2.4 GHz, there was three erroneous decision (subject 6, 7 and 18) in prone and side posture assessment and using $T_{A2} = 0.53$ for 5.8 GHz, there were in total six erroneous decisions (subjects 6, 7, 9, 11, 17, 20) for supine, prone and side posture assessment of twenty subjects. Here, it should be mentioned that new thresholds were fit on the twenty subjects dataset whereas the old threshold was applicable for 18 subjects. The percentage of subjects for which all postures were recognized correctly was calculated as 90% for 2.4 GHz and 80% for 5.8 GHz, as illustrated in Fig. 9.

While the results for 2.4 GHz were most promising, the complementary nature of the limitations for each frequency suggested a dual-frequency decision algorithm could produce more accurate decisions than for either frequency alone. A dual-frequency algorithm was developed, shown in Fig. 7(b), which applies the ratio threshold tests to both frequencies and expands the process to introduce a third set of thresholds for the arc radius ratios. The additional arc radius ratio thresholds used were $T_{A3} = 1.25$ for 2.4 GHz, and $T_{A3} = 0.7$ for 5.8 GHz. Where arc ratios required dual-frequency combinations (Fig. 7(b)), the distinct arc ratios are indicated with a 2.4 or 5.8 subscript denoting the corresponding frequency in GHz. As illustrated in Fig. 9 (confusion matrix), postures for 18 out of 18 subjects (100%) were correctly assessed using the dual-frequency measurement. It is expected that each single-frequency improvement from the arc length interquartile range will make the dual-frequency assessment accuracy more robust for larger, more disperse data sets. The benefits of frequency diversity and the particular selection of operating wavelengths were based on three factors [36]:

The wavelength of choice must satisfy the conditions of far-field measurements for accurate detection of a given target. On one hand, the radiation far-field condition requires the target to be placed at a distance covering multiple wavelengths. On the other hand, for a fixed target size d, the plane wave incidence condition requires the target range to be larger than $2d^2/\lambda$. This implies higher frequencies will require the target to be placed at further distances. Since this radar is intended to assess patients lying in bed, the target range is limited by the size of the room. The achievable range would typically be within 2m, assuming the antennas would be attached to the ceiling. Applying the equation above with 2.4-GHz and 5.8-GHz carriers, the radar illuminates a far-field target with a diameter sweeping from 23 cm to 35 cm [36]. This aligns with the expected target size in this application where the ERCS can vary from supine/prone posture to fetal posture.

The Mie relation of RCS for spherical targets shows that the RCS is a function of the operating wavelength. If the incident frequency is such that the target falls in the resonance region of wave scattering, the RCS presented by the target fluctuates with the target size. This will represent a challenge when comparing two unknown targets with different sizes. The operating wavelength must be small with respect to the circumference of the physical cross-section of the target to place the latter in the optical region where the RCS monotonically increases with the target size. At 2.4 GHz, the average human torso lies toward the end of the resonance region, while for 5.8 GHz the target is deeper in the desired optical region [36].

The third factor that determines the wavelength choice is the target displacement magnitude. The human torso displacement with respiration translates into an angle scanned by the arc in the center-estimation algorithm. For accurate estimation of the circle center, an arc scanning between 30 and 60 degrees is desired. With a 2.4-GHz operating frequency, the optimum target displacement will be from 1 cm to 2 cm; while for 5.8 GHz, it will be from 0.5 cm to 1 cm. This aligns with the expected window of average human torso displacement [36].

In summary, by having two transmitters illuminating the target with two separate frequencies, the received signals can be processed separately and hence improve the overall system performance. The choice of 2.4 GHz and 5.8 GHz is optimum for the specific application of the radar, in terms of target properties and the placement of the radar. Frequencies lower than 2.4 GHz would be deeper in the resonance region of wave scattering and would result in smaller scanning angles with torso displacement. Frequencies above 5.8 GHz would require a greater distance for the target to satisfy the far-field condition and could lead to phase-wrapping issues with larger torso displacements [48]. While the thresholds were based on average statistical trends observed in the data that was subsequently used for validation, the fact that the system ultimately accommodated all outliers is noteworthy.

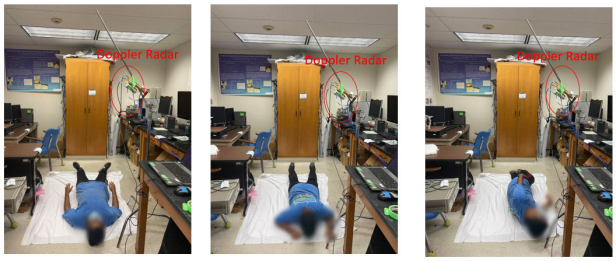

FIGURE 10. Experimental scenario in an office environment where the participant switches postures each minute between supine (a), prone (b), and side (c).

The design criteria for selecting thresholds were based on observations and statistical trends in the dataset. Additionally, the box-plot analysis provided insight on data distribution for different postures. For refining the threshold, the interquartile range (IR) of the data set was used which provides insight on the upper and lower limit variations. For example, initially, $T_{A2} = 0.5$ was tried for 2.4 GHz, but replacing that number with the interquartile range of 1.25 increased the accuracy of the single-frequency algorithm. In summary, some thresholds were selected based on observation and some were selected based on statistical trends.

This demonstrates that the proposed dual-band Doppler radar system can efficiently differentiate between the three sleep-type postures of a patient while monitoring cardiopulmonary activity. Since the algorithm requires initial values only in the supine posture, and since no absolute ERCS reading is needed, a minimum burden is imposed for both the patient and the clinic specialist. The latter can conveniently take the reference readings once the patient is in bed and does not have to go through any calibration process for the other two postures.

VI. COMMON ENVIRONMENT ALGORITHM VALIDATION

To test the efficacy of the proposed system and algorithm in a realistic setting, postures were also measured in an office environment. Fig. 10 illustrates the experimental scenario where the Doppler radar system was mounted on the ceiling and the subject reclined on a flat horizontal surface 2.15 m beneath it. A total of three repetitive measurements were taken. The subject started in the supine posture for one minute and then switched to the prone and side postures. Fig. 11 illustrates the radar-captured breathing patterns during sleep for the three different postures. In the time-domain signal, there was an abrupt change during switching of postures. The captured time-domain signal was analyzed to extract the relative ERCS and the absolute torso displacement magnitude. A segmentation technique was used to remove the abrupt spikes during posture transition [49]. In the segmentation technique, 60% of the maximum amplitude was discarded and the rest of the periodic signal was analyzed. Each segment traced an arc on the complex I-Q plot shown in Fig. 11 (b) where the radius of the arc was estimated using a center estimation and circle fitting algorithm [32]. For 2.4 GHz, supine, prone, and

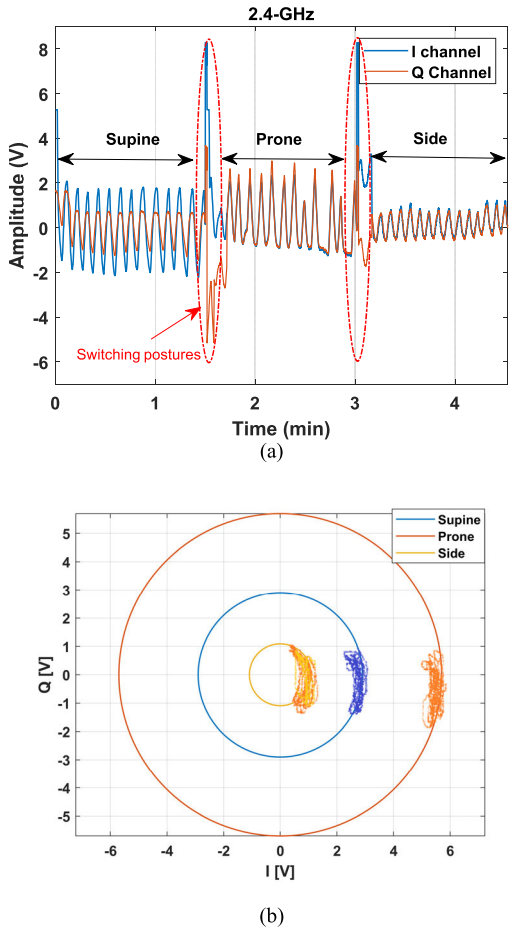

FIGURE 11. Data for subject in three different sleep postures, taken in an office environment. Posture change events are evident in the time-domain plot (a) where red ellipses highlight the transition from one posture to another. In the arc-radius estimation from the I/Q plo (b), prone postures result in the highest arc-radius, around 5.71 V.

side postures the relative ERCS or arc radius was 2.90, 5.70, and 1.09, respectively, as shown in Fig. 10 (b). Similarly, the chest displacement magnitudes were extracted for different postures from the recorded dataset. The chest displacement information for supine, prone, and side postures was 1.14cm, 0.43 cm, and 0.53 cm, respectively. From the ratios of ERCS and chest breadth measurements, the proposed single and dual-frequency algorithms were applied and accurately recognized the three different postures using the thresholds established in the initial anechoic chamber study. While this experiment which took place in an office environment with no rf control clearly illustrates anecdotal efficacy, further testing in the home or hospital environments should be conducted to identify potential interference and anomalies before collecting long-term data for related clinical applications.

VII. CONCLUSION

A dual-frequency Doppler radar system that integrates sleep posture recognition with cardiopulmonary monitoring has been successfully demonstrated, with measurement results for a 20-subject human study analyzed for the recognition of three critical categories of imitated sleep postures. The approach used is uniquely based on a physical model that does not require subject-specific supervised training with monitoring data for each posture to be recognized.

It has been shown that the properties of the baseband signals at the radar receiver depend on the orientation of the subject with respect to the viewpoint of the transceiver antennas. The ability to discriminate between these properties for different orientations is key to monitoring the posture of the subject by remote sensing using Doppler radar. With the baseband signal represented as quadrature components, digital processing algorithms were applied to extract the ERCS and displacement magnitude of the torso during respiration. Measurements of metallic spherical targets, modeling expected human respiratory motion, indicated that these two quantities can be effectively measured within acceptable accuracy.

To explore the relation between the measured parameters at different orientations, human testing was performed on a sample group of twenty subjects. By comparing the ERCS values and displacement magnitudes measured for three sleep postures, some trends were clearly observed. For all collected data, results obtained in supine posture were taken as a reference, emulating the practical case where measurements could be first taken in the supine posture. The ERCS obtained in the prone posture was ultimately greater than that in supine for measurements performed at 2.4 GHz. This observation was less prominent for the 5.8 GHz system due to the spherical property of the incident wave at the relatively short target range, which leads to a reduction in sensitivity to target curvature.

On the contrary, the effective ERCS in the side posture was smaller than that in supine for most subjects at both 2.4 and 5.8 GHz. The latter showed larger discrepancy between the two postures as the target extends toward the optical region of electromagnetic scattering. In that region, the ERCS is directly proportional to the physical cross section and since the size of the body side is smaller than the front or back, a smaller ERCS is expected.

Additionally, the change in sleep posture compared to prone was associated with a reduction in respiration depth with respect to supine. This was observed for both operating frequencies and the reduction consistently averaged out to about 50%. For the side posture, the displacement magnitude was comparable to that in supine and was only 20% less on average.

Based on the statistical analyses of the population of subjects, and considering the tolerances in measurements, a decision algorithm was developed to investigate the potential to identify a subject's orientation from the measured ERCS and torso displacement magnitude. Having data only for the known supine posture, the algorithm successfully worked for all eighteen subjects with valid data. This work concentrated on recognizing three different generalized sleep postures (supine, prone, and side). Each subject assumed the postures in their own way. In principle, recognition of additional intermediate sleep-related postures can be similarly

attained using Doppler radar and remains beyond the scope of this study.

The proposed method successfully tracked three distinct recumbent postures for a twenty-person study in an anechoic chamber, with an additional successful tracking demonstration made in an office environment. As no two people assumed the exact same form of each posture, there is some level of robustness in our classifications that should hold up whether or not the subject is asleep. A full clinical study with a large sample of sleeping subjects, and simultaneous video and polysomnography reference measurements, would be an important step in bringing this posture measurement technique to practical use.

REFERENCES

[1] M. Kryger, T. Roth, and W. Dement, *Principles and Practice of Sleep Medicine*, Amsterdam, The Netherlands: Elsevier, 2017.

[2] K. L. Knutson and E. Van Cauter, "Associations between sleep loss and increased risk of obesity and diabetes," *Ann. New York Acad. Sci.*, vol. 1129, no. 1, pp. 287–304, May 2008, doi: 10.1196/annals.1417.033.

[3] J. R. Tietjens, D. Claman, E. J. Kezirian, T. De Marco, A. Mirzayan, B. Sadroonri, A. N. Goldberg, C. Long, E. P. Gerstenfeld, and Y. Yeghiazarians, "Obstructive sleep apnea in cardiovascular disease: A review of the literature and proposed multidisciplinary clinical management strategy," *J. Amer. Heart Assoc.*, vol. 8, no. 1, Jan. 2019, Art. no. e010440, doi: 10.1161/JAHA.118.010440.

[4] I. Soreca, J. Levenson, M. Lotz, E. Frank, and D. Kupfer, "Sleep apnea risk and clinical correlates in patients with bipolar disorder," *Bipolar Disorders*, vol. 14, vol. 6, pp. 672–676, 2012, doi: 10.1111/j.1399-5618.2012.01044.x.

[5] M. Marques, P. R. Genta, S. A. Sands, A. Azarbazin, C. de Melo, L. Taranto-Montemurro, D. P. White, and A. Wellman, "Effect of sleeping position on upper airway patency in obstructive sleep apnea is determined by the pharyngeal structure causing collapse," *Sleep*, vol. 40, no. 3, Mar. 2017, Art. no. zsx005, doi: 10.1093/sleep/zsx005.

[6] J. Liu, X. Chen, S. Chen, X. Liu, Y. Wang, and L. Chen, "TagSheet: Sleeping posture recognition with an unobtrusive passive tag matrix," in *Proc. IEEE Conf. Comput. Commun.*, Paris, France, Apr. 2019, pp. 874–882, doi: 10.1109/INFOCOM.2019.8737599.

[7] X. Xu, F. Lin, A. Wang, C. Song, Y. Hu, and W. Xu, "On-bed sleep posture recognition based on body-Earth mover's distance," in *Proc. IEEE Biomed. Circuits Syst. Conf. (BioCAS)*, Atlanta, GA, USA, Oct. 2015, pp. 1–4, doi: 10.1109/BioCAS.2015.7348281.

[8] Z. Zhang and G.-Z. Yang, "Monitoring cardio-respiratory and posture movements during sleep: What can be achieved by a single motion sensor," in *Proc. IEEE 12th Int. Conf. Wearable Implant. Body Sensor Netw. (BSN)*, Cambridge, MA, USA, Jun. 2015, pp. 1–6, doi: 10.1109/BSN.2015.7299409.

[9] S. Zhang, G. Wang, and X. Guo, "Sleep-pose recognition based on pyroelectric infrared sensing technology," in *Proc. 13th World Congr. Intell. Control Autom. (WCICA)*, Changsha, China, Jul. 2018, pp. 495–498, doi: 10.1109/WCICA.2018.8630453.

[10] A. Oksenberg and D. S. Silverberg, "Avoiding the supine posture during sleep for patients with mild obstructive sleep apnea," *Amer. J. Respiratory Crit. Care Med.*, vol. 180, no. 1, p. 101, Jul. 2009, doi: 10.1164/ajrccm.180.1.101a.

[11] N. Goldberg, Y. Rodriguez-Prado, R. Tillery, and C. Chua, "Sudden infant death syndrome: A review of the medical literature 1974-1979," *Pediatrics Ann.*, vol. 47, no. 3, pp. e118–e123, 2018, doi: 10.3928/19382359-20180221-03.

[12] K. D. Duncan, "Preventing pressure ulcers: The goal is zero," *Joint Commission J. Qual. Patient Saf.*, vol. 33, no. 10, pp. 605–610, Oct. 2007, doi: 10.1016/S1553-7250(07)33069-9.

[13] H. J. Lee, S. H. Hwang, S. M. Lee, Y. G. Lim, and K. S. Park, "Estimation of body postures on bed using unconstrained ECG measurements," *IEEE J. Biomed. Health Informat.*, vol. 17, no. 6, pp. 985–993, Nov. 2013, doi: 10.1109/JBHI.2013.2252911.

[14] T. Grimm, M. Martinez, A. Benz, and R. Stiefelhagen, "Sleep position classification from a depth camera using Bed Aligned Maps," in *Proc. 23rd Int. Conf. Pattern Recognit. (ICPR)*, Cancun, Mexico, Dec. 2016, pp. 319–324, doi: 10.1109/ICPR.2016.7899653.

[15] S. Ostadabbas, M. Baran Pouyan, M. Nourani, and N. Kehtarnavaz, "In-bed posture classification and limb identification," in *Proc. IEEE Biomed. Circuits Syst. Conf. (BioCAS)*, Lausanne, Switzerland, Oct. 2014, pp. 133–136, doi: 10.1109/BioCAS.2014.6981663.

[16] C. Li, V. M. Lubecke, O. Boric-Lubecke, and J. Lin, "A review on recent advances in Doppler radar sensors for noncontact healthcare monitoring," *IEEE Trans. Microw. Theory Techn.*, vol. 61, no. 5, pp. 2046–2060, May 2013.

[17] A. D. Droitcour, T. B. Seto, B.-K. Park, S. Yamada, A. Vergara, C. El Hourani, T. Shing, A. Yuen, V. M. Lubecke, and O. Boric-Lubecke, "Non-contact respiratory rate measurement validation for hospitalized patients," in *Proc. Annu. Int. Conf. IEEE Eng. Med. Biol. Soc.*, Minneapolis, MN, USA, Sep. 2009, pp. 4812–4815, doi: 10.1109/IEMBS.2009.5332635.

[18] Y. Yuan, C. Lu, A. Y.-K. Chen, C.-H. Tseng, and C.-T.-M. Wu, "Multi-target concurrent vital sign and location detection using metamaterial-integrated self-injection-locked quadrature radar sensor," *IEEE Trans. Microw. Theory Techn.*, vol. 67, no. 12, pp. 5429–5437, Dec. 2019, doi: 10.1109/TMTT.2019.2931834.

[19] W.-C. Su, M.-C. Tang, R. E. Arif, T.-S. Horng, and F.-K. Wang, "Stepped-frequency continuous-wave radar with self-injection-locking technology for monitoring multiple human vital signs," *IEEE Trans. Microw. Theory Techn.*, vol. 67, no. 12, pp. 5396–5405, Dec. 2019, doi: 10.1109/TMTT.2019.2933199.

[20] S. M. M. Islam, O. Boric-Lubecke, and V. M. Lubekce, "Concurrent respiration monitoring of multiple subjects by phase-comparison monopulse radar using independent component analysis (ICA) with JADE algorithm and direction of arrival (DOA)," *IEEE Access*, vol. 8, pp. 73558–73569, 2020, doi: 10.1109/ACCESS.2020.2988038.

[21] V. P. Tran, A. A. Al-Jumaily, and S. M. S. Islam, "Doppler radar-based non-contact health monitoring for obstructive sleep apnea diagnosis: A comprehensive review," *Big Data Cognit. Comput.*, vol. 3, no. 1, p. 3, Jan. 2019, doi: 10.3390/bdcc3010003.

[22] M. Zakrzewski, A. Vehkaoja, A. S. Joutsen, K. T. Palovuori, and J. J. Vanhala, "Noncontact respiration monitoring during sleep with microwave Doppler radar," *IEEE Sensors J.*, vol. 15, no. 10, pp. 5683–5693, Oct. 2015, doi: 10.1109/JSEN.2015.2446616.

[23] F. Lin, Y. Zhuang, C. Song, A. Wang, Y. Li, C. Gu, C. Li, and W. Xu, "SleepSense: A noncontact and cost-effective sleep monitoring system," *IEEE Trans. Biomed. Circuits Syst.*, vol. 11, no. 1, pp. 189–202, Feb. 2017, doi: 10.1109/TBCAS.2016.2541680.

[24] T. Rahman, A. T. Adams, R. V. Ravichandran, M. Zhang, S. N. Patel, J. A. Kientz, and T. Choudhury, "DoppleSleep: A contactless unobtrusive sleep sensing system using short-range Doppler radar," in *Proc. ACM Int. Joint Conf. Pervas. Ubiquitous Comput.*, Osaka, Japan, 2015, pp. 39–50, doi: 10.1145/2750858.2804280.

[25] M. Baboli, A. Singh, B. Soll, O. Boric-Lubecke, and V. M. Lubecke, "Wireless sleep apnea detection using continuous wave quadrature Doppler radar," *IEEE Sensors J.*, vol. 20, no. 1, pp. 538–545, Jan. 2020, doi: 10.1109/JSEN.2019.2941198.

[26] K. Van Loon, M. J. M. Breteler, L. Van Wolfwinkel, A. T. Rheineck Leyssius, S. Kossen, C. J. Kalkman, B. Van Zaane, and L. M. Peelen, "Wireless non-invasive continuous respiratory monitoring with FMCW radar: A clinical validation study," *J. Clin. Monitor. Comput.*, vol. 30, no. 6, pp. 797–805, Dec. 2016, doi: 10.1007/s10877-015-9777-5.

[27] M. Alizadeh, G. Shaker, J. C. M. D. Almeida, P. P. Morita, and S. Safavi-Naeini, "Remote monitoring of human vital signs using mm-wave FMCW radar," *IEEE Access*, vol. 7, pp. 54958–54968, 2019, doi: 10.1109/ACCESS.2019.2912956.

[28] S. Toften, S. Pallesen, M. Hrozanova, F. Moen, and J. Grønli, "Validation of sleep stage classification using non-contact radar technology and machine learning (Somnofy)," *Sleep Med.*, vol. 75, pp. 54–61, Nov. 2020, doi: 10.1016/j.sleep.2020.02.022.

[29] Y. Zhou, D. Shu, H. Xu, Y. Qiu, and P. Zhou, "Validation of novel automatic ultra-wideband radar for sleep apnea detection," *J. Thoracic Disease*, vol. 12, no. 4, pp. 1286–1295, 2020, doi: 10.21037/jtd.2020.02.5.

[30] V. P. Tran and A. A. Al-Jumaily, "Non-contact Doppler radar based prediction of nocturnal body orientations using deep neural network for chronic heart failure patients," in *Proc. Int. Conf. Electr. Comput. Technol. Appl. (ICECTA)*, Ras Al Khaimah, United Arab Emirates, Nov. 2017, pp. 1–5, doi: 10.1109/ICECTA.2017.8252020.

[31] S. Yue, Y. Yang, H. Wang, H. Rahul, and D. Katabi, "BodyCompass: Monitoring sleep posture with wireless signals," *ACM Interact. Mob. Wearable Ubiquitous Technol.*, vol. 4, no. 2, pp. 1–25, Jun. 2020, doi: 10.1145/3397311.

[32] J. E. Kiriazi, O. Boric-Lubecke, and V. M. Lubecke, "Dual-frequency technique for assessment of cardiopulmonary effective RCS and displacement," *IEEE Sensors J.*, vol. 12, no. 3, pp. 574–582, Mar. 2012, doi: 10.1109/JSEN.2011.2124454.

[33] W. Massagram, N. Hafner, V. Lubecke, and O. Boric-Lubecke, "Tidal volume measurement through non-contact Doppler radar with DC reconstruction," *IEEE Sensors J.*, vol. 13, no. 9, pp. 3397–3404, 2013, doi: 10.1109/JSEN.2013.2257733.

[34] A. Singh, V. Lubecke, and O. Boric-Lubecke, "Pulse pressure monitoring through non-contact cardiac motion detection using 2.45 GHz microwave Doppler radar," in *Proc. Annu. Int. Conf. IEEE Eng. Med. Biol. Soc.*, Boston, MA, USA, Aug. 2011, pp. 4336–4339, doi: 10.1109/IEMBS.2011.6091076.

[35] F. Snigdha, S. M. M. Islam, and O. Boric-Lubecke, "Obstructive sleep apnea events classification by effective radar cross section (ERCS) method by using microwave Doppler Radar and machine learning classifiers," in *IEEE MTT-S Int. Microw. Symp. Dig.*, Toulouse, France, Dec. 2020.

[36] J. E. Kiriazi, "Human cardiopulmonary recognition using close-range Doppler radar," Ph.D. dissertation, Univ. Hawaii Manoa, Honolulu, HI, USA, Dec. 2010.

[37] J. E. Kiriazi, O. Boric-Lubecke, and V. M. Lubecke, "Considerations in measuring vital signs cross section with Doppler radar," in *Proc. IEEE Radio Wireless Symp.*, Phoenix, AZ, USA, Jan. 2011, pp. 426–429, doi: 10.1109/RWS.2011.5725515.

[38] C. Gu and C. Li, "DC coupled CW radar sensor using fine-tuning adaptive feedback loop," *Electron. Lett.*, vol. 48, no. 6, pp. 344–345, Mar. 2012.

[39] E. F. Knott, J. F. Shaeffer, and M. T. Tuley, *Radar Cross Section*, 2nd ed. Norwood, MA, USA: Artech House, 1993.

[40] B. K. Park, V. M. Lubecke, O. Boric-Lubecke, and A. Host-Madsen, "Center tracking quadrature demodulation for a Doppler radar motion detector," in *Proc. IEEE Intern. Microw. Symp.*, Honolulu, HI, USA, Jun. 2007, pp. 1323–1326.

[41] S. R. de Gauna, D. M. González-Otero, J. Ruiz, and J. K. Russell, "Feedback on the rate and depth of chest compressions during cardiopulmonary resuscitation using only accelerometers," *PLoS ONE*, vol. 11, no. 3, Mar. 2016, Art. no. e0150139, doi: 10.1371/journal.pone.0150139.

[42] G. Benchetrit, "Breathing pattern in humans: Diversity and individuality," *Respirat. Physiol.*, vol. 122, nos. 2–3, pp. 123–129, Sep. 2000, doi: 10.1016/S0034-5687(00)00154-7.

[43] C. Li and J. Lin, "Random body movement cancellation in Doppler radar vital sign detection," *IEEE Trans. Microw. Theory Techn.*, vol. 56, no. 12, pp. 3143–3152, Dec. 2008, doi: 10.1109/TMTT.2008.2007139.

[44] C. Gu, G. Wang, T. Inoue, and C. Li, "Doppler radar vital sign detection with random body movement cancellation based on adaptive phase compensation," in *IEEE MTT-S Int. Microw. Symp. Dig.*, Seattle, WA, USA, Jun. 2013, pp. 1–3, doi: 10.1109/MWSYM.2013.6697618.

[45] C. Gu, G. Wang, Y. Li, T. Inoue, and C. Li, "A hybrid radar-camera sensing system with phase compensation for random body movement cancellation in Doppler vital sign detection," *IEEE Trans. Microw. Theory Techn.*, vol. 61, no. 12, pp. 4678–4688, Dec. 2013, doi: 10.1109/TMTT.2013.2288226.

[46] W. Massagram, V. M. Lubecke, A. Host-Madsen, and O. Boric-Lubecke, "Assessment of heart rate variability and respiratory sinus arrhythmia via Doppler radar," *IEEE Trans. Microw. Theory Techn.*, vol. 57, no. 10, pp. 2542–2549, Oct. 2009, doi: 10.1109/TMTT.2009.2029716.

[47] J. E. Kiriazi, O. Boric-Lubecke, and V. M. Lubecke, "Modeling of human torso time-space characteristics for respiratory effective RCS measurements with Doppler radar," in *IEEE MTT-S Int. Microw. Symp. Dig.*, Baltimore, MD, USA, Jun. 2011, pp. 1–4, doi: 10.1109/MWSYM.2011.5972881.

[48] S. M. M. Islam, N. Motoyama, S. Pacheco, and V. M. Lubecke, "Non-contact vital signs monitoring for multiple subjects using a millimeter wave FMCW automotive radar," in *IEEE MTT-S Int. Microw. Symp. Dig.*, Los Angeles, CA, USA, Aug. 2020, pp. 783–786, doi: 10.1109/IMS30576.2020.9223838.

[49] S. M. M. Islam, A. Sylvester, G. Orpilla, and V. M. Lubecke, "Respiratory feature extraction for radar-based continuous identity authentication," in *Proc. IEEE Radio Wireless Symp. (RWS)*, San Antonio, TX, USA, Jan. 2020, pp. 119–122, doi: 10.1109/RWS45077.2020.9050013.

JOHN E. KIRIAZI (Member, IEEE) received the B.Sc. and M.S. degrees in electrical engineering from Ain Shams University, Cairo, Egypt, in 2001 and 2005, respectively, and the Ph.D. degree in electrical engineering from the University of Hawaii at Manoa, Honolulu, in 2010.

From 2001 to 2005, he was a Demonstrator with the Department of Electronics and Communications, Ain Shams University, where his research focused on reconfigurable planar antennas and micro-electromechanical systems technology. Since 2009, he has been with Qualcomm Inc., San Diego, CA, USA, where he joined the RF Systems Group and has contributed to the development of RF devices spanning multi generations of cellular technology.

He is currently with the RFFE Team, RF Systems Group, Qualcomm Inc., leading the development and commercialization of state-of-the-art frontend devices for 5G mobile communication systems. His academic research interests include microwave remote sensing and biomedical applications.

SHEKH M. M. ISLAM (Member, IEEE) received the B.Sc. (Hons.) and M.Sc. degrees in electrical and electronic engineering from the University of Dhaka, Dhaka, Bangladesh, in 2012 and 2014, respectively, and the Ph.D. degree in electrical engineering from the University of Hawaii at Manoa, Honolulu, HI, USA, with a focus on biomedical applications incorporating RF/microwave technologies in 2020.

From 2014 to 2016, he was a Lecturer with the Department of Electrical and Electronic Engineering, University of Dhaka. His research interests include radar systems, antenna array signal processing, adaptive filter technique, and machine learning classifiers for pattern recognition. In 2019, he was also a Radar System and Applications Engineering Intern with ON Semiconductor, Phoenix, AZ, USA.

Dr. Islam is also an active member of the IEEE Microwave Theory and Technique and the IEEE Engineering in Medicine and Biology societies. He was a recipient of the 2020 University of Hawaii at Manoa Department of Electrical Engineering Research Excellence Award. He was also the Student Paper Finalist at the IEEE Radio Wireless Week (RWW'19) Conference, which was held in FL, USA. He has also been serving as a review editor of the *MDPI Sensor*, *Frontiers in Sensors*, and *Frontiers in Communication and Network* journals.

OLGA BORIĆ-LUBECKE (Fellow, IEEE) received the B.Sc. degree from the University of Belgrade, Belgrade, Yugoslavia, in 1989, the M.S. degree from the California Institute of Technology, Pasadena, CA, USA, in 1990, and the Ph.D. degree from the University of California at Los Angeles, in 1995, all in electrical engineering.

Since 2003, she has been with the University of Hawaii (UH) at Manoa, Honolulu, HI, USA, where she is currently a Professor of electrical engineering. From 1995 to 1996, she was a Resident Research Associate with the NASA Jet Propulsion Laboratory, Pasadena. From 1996 to 1998, she was a Visiting Researcher with the Institute of Physical and Chemical Research, Sendai, Japan. She was with Bell Laboratories, Lucent Technologies, Murray Hill, NJ, USA, where she conducted research in RF integrated circuit technology and biomedical applications of wireless systems. She has authored over 200 journal and conference publications, two books, and several book chapters. Her research has been featured by various media outlets. She has two patents. Her current research interests include RF and high-frequency integrated circuits, wireless systems, biomedical applications, and renewable energy.

She co-founded and served as the Chief Technical Advisor for a start-up company, Kai Medical. She is also a Co-Founder and the President of Adnoviv, Inc. She is currently an IEEE Microwave Theory and Techniques (MTT) Fellow Selection Committee Member. She is a Distinguished Member of the National Academy of Inventors, UH Chapter. She is also a Foreign Member of the Academy of Engineering of Serbia. She was a co-recipient of the Emerging Technology Award at TechConnect 2007. She was the adviser author of several award-winning IEEE MTT Society and IEEE Engineering in Medicine and Biology Society (EMB) student papers. She has served as the Workshop Chair for the 2003 IEEE IMS, the Technical Program Vice Chair for the 2007 IEEE IMS, and the Technical Program Co-Chair for the 2017 IEEE IMS, and the 2018 IEEE IMS Technical Program Advisor. She has served as an Associate Editor for the IEEE Microwave and Wireless Components Letters from 2012 to 2015 and the IEEE Transactions on Microwave Theory and Techniques from 2015 to 2017. She currently serves as an IEEE EMBC Associate Editor.

VICTOR M. LUBECKE (Fellow, IEEE) received the B.S.E.E. degree from the California Polytechnic Institute, Pomona, in 1986, and the M.S. and Ph.D. degrees in electrical engineering from the California Institute of Technology, Pasadena, in 1990 and 1995, respectively. He is currently a Professor of electrical engineering with the University of Hawai'i, Mānoa, HI, USA. From 1998 to 2003, he was with Bell Laboratories, Lucent Technologies, where his research focused on remote sensing technologies for biomedical and industrial applications, and on microelectromechanical systems and 3-D wafer-scale integration technologies for wireless and optical communications.

From 1987 to 1996, he was with the NASA Jet Propulsion Laboratory and from 1996 to 1998, he was with the Institute for Physical and Chemical Research, Sendai, Japan, where his research involved terahertz and MEMS technologies for space remote sensing and communications applications. He holds seven U.S. patents with several pending. He has authored or coauthored hundreds of peer-reviewed research articles.

He co-founded two technology start-up companies. His current research interests include remote sensing technologies, biomedical sensors, microwave/terahertz radio, and MEMS, heterogeneous integration. He is an emeritus Distinguished Microwave Lecturer of the IEEE Microwave Theory and Techniques Society from 2006 to 2008. He served as a Topic Editor for the IEEE Transactions on Terahertz Science and Technology. He is also a member of the IEEE Engineering in Medicine and Biology and Electron Devices societies and serves on Technical Committees for Terahertz Technology and Applications and Biological Effects and Medical Applications. He has also served on steering committees for various IEEE and SPIE committees and symposia, including the Vice Chair for the 2017 IEEE International Microwave Symposium. He was a recipient of the 2000 Microwave Prize for Best Paper Award presented at the Asia–Pacific Microwave Conference. He has several student paper awards at the IEEE conferences. He was a co-recipient of the Emerging Technology Award at TechConnect 2007.